Power Control Strategies for Single-Phase Voltage-Controlled Inverters with an Enhanced PLL

Jiayuan Gao[*], Jinbin Zhao[†], Chaojie He[*], Shuaitao Zhang[*], and Fen Li[*]

[*],[†]College of Electrical Engineering, Shanghai University of Electric Power, Shanghai, China

Abstract

For maintaining a reliable and secure power system, this paper describes the design and implement of a single-phase grid-connected inverter with an enhanced phase-locked loop (PLL) and excellent power control performance. For designing the enhanced PLL and power regulator, a full-bridge voltage-controlled inverter (VCI) is investigated. When the grid frequency deviates from its reference values, the output frequency of the VCI is unstable with an oscillation of 2 doubling harmonics. The reason for this oscillation is analyzed mathematically. This oscillation leads to an injection of harmonics into the grid and even causes an output active power oscillation of the VCI. For eliminating the oscillation caused by a PLL, an oscillation compensation method is proposed. With the proposed method, the VCI maintains the original PLL control characteristics and improves the PLL robustness under grid frequency deviations. On the basis of the above analysis, a power regulator with the primary frequency and voltage modulation characteristics is analyzed and designed. Meanwhile, a small-signal model of the power loops is established to determine the control parameters. The VCI can accurately output target power and has primary frequency and voltage modulation characteristics that can provide active and reactive power compensation to the grid. Finally, simulation and experimental results are given to verify the idea.

Key words: 2 doubling harmonics, Grid-connected operation, Phase-locked loop, Power oscillation, Primary frequency, Voltage modulation, Voltage-controlled inverter

I. INTRODUCTION

As one of the most substantial sources of growth in terms of power generation, renewable energy utilized via power electronics converters is confronted with significant challenges for maintaining reliable and secure operation of a power system [1], [2]. Distributed generation (DG) systems based on renewable energy sources can supply active and reactive power to loads in both standalone and grid-connected operations [3]-[5]. However, the basic performances of conventional power conversion systems are different from those of conventional synchronous generators (SG), which can follow both loads and malfunction fluctuations autonomously in a utility grid with automatic voltage regulation and governor system operation [6]. To maintain the power supply quality in a grid, the grid needs to provide relatively expensive ancillary services to suppress vast disturbances.

An inverter equipped with both control and synchronization strategies is always controlled as an ac current source to inject active and reactive power into the grid [7]-[9]. When the point of common coupling (PCC) voltage and frequency seriously deviate from the default value, the reliable and secure operation of the power system is affected. With the high penetration of renewable energy, mismatches between the input and output power of the grid cause serious deviation of the PCC voltage and frequency [10], [11]. If the inverter can operate in a similar manner as a SG with the primary frequency and voltage modulation [12], the standalone and integrated operation control system of the DG system becomes simpler and more integrated.

While the inverter is controlled as a current supply, the key techniques are the detection of reactive power, acquisition of the grid-connected reference current, and grid current control for regulating the active and reactive power. When the penetration of renewable energy exceeds a certain level, it becomes difficult for a current-controlled inverter to take part in the essential regulation of the grid frequency and voltage [13]. When the inverter is controlled as a voltage supply, the
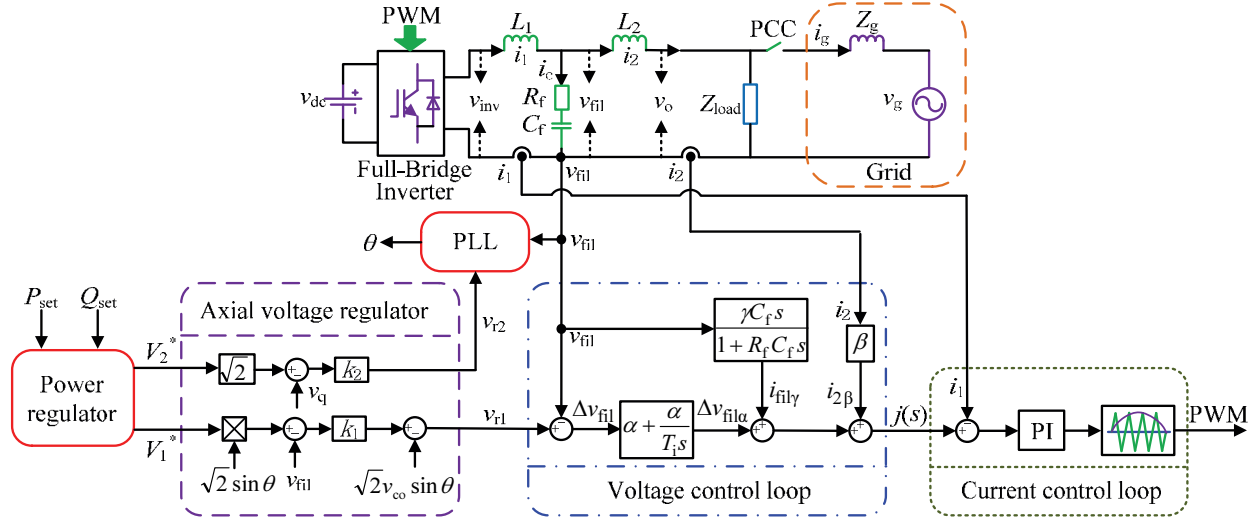
Fig. 1. Overview of the investigated configuration and control system for a VCI operated in the grid.

active and reactive power are regulated using the ac voltage angle and magnitude [14].

In a three-phase system, the power regulation can be conveniently controlled based on both the *dq* rotating synchronous reference frame and the instantaneous power theory [15]-[18]. In a single-phase system, the dq component needs to be synthesized using a 90° phase-shift operation at the fundamental frequency [19]-[21]. This 90° phase-shift operation can be performed by different methods such as the time-delay method, all-pass filter, Hilbert transform, second-order generalized integrator (SOGI), or enhanced phase-locked loop (EPLL) [22]-[25]. On the one hand, the long delay affects the system dynamic responses. On the other hand, the accuracy and availability of the 90° phase-shift operation influences the system control performance.

In this paper, the method of quarter cycle time-delay is used for acquisition of the *dq* component in the PLL. When the grid frequency deviates from the default value, the *dq* component has an undesired 2 doubling harmonics which directly leads the VCI output frequency oscillation. Moreover, this causes an output active power oscillation of the VCI and indirectly affects the power regulator stability. To eliminate this oscillation, a compensation method is proposed which only utilizes the existing VCI inner control signals to acquire accurate 2 doubling harmonics. It is a simple but very effective way to improve the VCI control performance.

On the basis of the above analysis, a power regulator is designed to realize the automatic management of the VCI output active and reactive power. The main objective is the injection of the rated active power. However, if necessary, it can also regulate certain active and reactive power outputs for supporting the grid. With the power closed-loop control, the VCI can accurately output target power. With the *P-f* and *Q-V* droop mechanism, it can realize the primary frequency and voltage modulation characteristics in the VCI. On the

basis of the VCI control strategy, a detailed small-signal model of the power loops is established for designing the control parameters.

The rest of this paper is organized as follows. In section II, a VCI control algorithm is introduced to establish the VCI grid-connected operation model. The improvement of the PLL, the detailed small-signal model establishment and the control parameters design of the power regulator are mathematically analyzed in section III. Simulation and experimental results are given in section IV, followed by some conclusions and discussions in section V.

II. OVERVIEW OF THE VCI GRID-CONNECTED MODEL

On the basis of the inverter control algorithm in [26], the VCI grid-connected model can be shown as Fig. 1.

The system control structure consists of a power regulator, PLL, axial voltage regulator, current control loop and voltage control loop. The axial voltage regulator block has two reference axial voltages V_1^* and V_2^*. In this block, V_1^* is used to adjust the voltage amplitude of the equivalent voltage source. Meanwhile, V_2^* is used to adjust the power angle between the equivalent voltage source and the inverter output voltage. k_1 and k_2 are the adjustment factors of the axial voltage. The outputs v_{r1} and v_{r2} of the axial voltage regulator are input to the voltage control and the PLL, respectively. The voltage control loop consists of 3 components, as shown in Fig. 1. These components are a voltage feedback loop with a PI controller, a feedforward component that is the inverter output current with the gain β added to the reference current $j(s)$, and a C_f current, which is compensated by adding its fundamental component to $j(s)$. Where α and T_i are the PI controller parameters, and γ is the current compensation coefficient of the C_f current. The current control serves as an
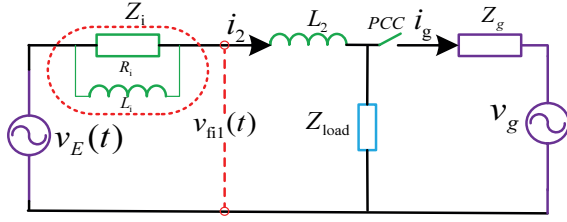
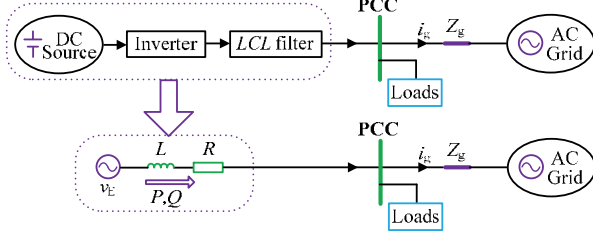Fig. 2 Grid-connected control equivalent model of a VCI.

Fig. 3. VCI grid-connected equivalent model.

inner loop with the SPWM modulation method, and the modulation gain factor can be seen as k_{PWM}.

Based on the relevant conclusions in [26], a grid-connected control equivalent model of a VCI is shown in Fig. 2. As a result, the grid-connected VCI as a voltage supply can easily take part in the regulation of the system frequency and voltage.

The VCI control characteristics can be obtained as:

$$v_E(t) = \sqrt{2}\,\frac{v_{co} + k_1 V_1^*}{1 + k_1}\sin\theta \qquad (1)$$

$$Z_i(s) = \frac{1 - \beta k_{PWM}}{(1 + k_1)\alpha k_{PWM}\left(1 + \dfrac{1}{T_i s}\right)} \qquad (2)$$

$$\delta = \left(\frac{1}{2\sqrt{2}\pi k_f(1 - k_2)V_{fil}} + \frac{\pi}{4\omega_{co}}\right)(\omega_{co} - \omega_g) + \frac{k_2}{(1 - k_2)V_{fil}}V_2^* \qquad (3)$$

Where v_{co} and ω_{co} are the VCI inner reference. In addition, ω_g is the grid angular frequency [rad/s], and δ is the phase shift between v_E and v_{fil}. The value θ is the output phase of the PLL. According to Eq. 2, the equivalent impedance Z_i in parallel form and the inductance L_2 can be equivalent to Z, where Z is equal to $R + Ls$.

On the basis of the VCI control characteristics, the VCI grid-connected model can be simplified as shown in Fig. 3. The VCI voltage amplitude and phase can be regulated by the axial voltages V_1^* and V_2^*, respectively. In grid-connected operation, the axial voltage V_1^* regulates the output reactive power whereas the axial voltage V_2^* regulates the output active power. It is easy to connect with a power grid since the VCI works as a small power station.

III. DESIGN OF THE PLL AND POWER REGULATOR

A. The Analysis of the Enhanced PLL

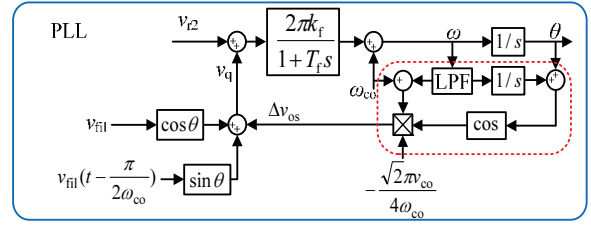For enhancing the stability of the VCI operation during

Fig. 4. Detailed control structure of the enhanced PLL.

grid frequency transients over a wide timeframe, the PLL operating characteristic are analyzed. Since the realization of the VCI governor-free characteristic is based on the acquisition of the v_{fil} dq component, the accuracy of the time-delay method concerns the PLL control performance. The control structure of the enhanced PLL, marked in the red frame, is shown in Fig. 4.

Firstly, suppose that the inverter connects with a stiff grid and that the capacitor voltage of the filter $v_{fil}(t)$ is expressed as:

$$v_{fil}(t) = \sqrt{2}V_{fil}\sin\omega_g t \qquad (4)$$

Then, the following equation is rearranged as:

$$v_{fil}\left(t - \frac{\pi}{2\omega_{co}}\right) \equiv -\sqrt{2}V_{fil}\cos\left(\frac{\pi(\omega_{co} - \omega_g)}{2\omega_{co}}\right)\cdot\cos\omega_g t$$
$$+ \sqrt{2}V_{fil}\sin\left(\frac{\pi(\omega_{co} - \omega_g)}{2\omega_{co}}\right)\cdot\sin\omega_g t \qquad (5)$$

In general, the deviation between ω_{co} and ω_g is small, and Eq. 5 can be approximated as follows:

$$v_{fil}\left(t - \frac{\pi}{2\omega_{co}}\right) = \sqrt{2}V_{fil}\left[\frac{\pi(\omega_{co} - \omega_g)}{2\omega_{co}}\cdot\sin\omega_g t - \cos\omega_g t\right] \qquad (6)$$

Therefore, v_q is calculated as below:

$$v_q(t) = v_{fil}(t)\cos\theta + v_{fil}\left(t - \frac{\pi}{2\omega_{co}}\right)\sin\theta$$
$$= \sqrt{2}V_{fil}\left[\sin(\omega_g t - \theta) + \frac{\pi(\omega_{co} - \omega_g)}{4\omega_{co}}\cos(\omega_g t - \theta)\right. \qquad (7)$$
$$\left. - \frac{\pi(\omega_{co} - \omega_g)}{4\omega_{co}}\cos(\omega_g t + \theta)\right]$$

On the basis of the PLL control algorithm and neglecting the 3rd term in Eq. 7, the VCI output voltage angle $\theta(s)$ can be obtained as:

$$\theta(s) = \frac{\omega_{co} + 2\sqrt{2}\pi k_f k_2 V_2^*}{\{s + 2\sqrt{2}\pi k_f(1 - k_2)V_{fil}\}s}$$
$$+ \frac{2\sqrt{2}\pi k_f(1 - k_2)V_{fil}\left[\omega_g + \dfrac{\pi(\omega_{co} - \omega_g)}{4\omega_{co}}s\right]}{\{s + 2\sqrt{2}\pi k_f(1 - k_2)V_{fil}\}s^2} \qquad (8)$$

According to Eq. 8, the steady state value of the converter angular frequency is obtained as follows:

$$\lim_{t\to\infty}\frac{d\theta(t)}{dt} = \lim_{s\to +0}s^2\theta(s) = \omega_g \qquad [rad/s] \qquad (9)$$

This indicates that the inverter can synchronize with the grid. However, if ω_g deviates from ω_{co} to a certain extent, the 3rd term in Eq. 7 cannot be neglected. The VCI output frequency obviously oscillates around ω_g, which brings the 2 doubling harmonics injection into the grid. This is harmful to the inverter output power quality and jeopardizes the VCI stability. Meanwhile, it can be seen from Eq. 3 that the VCI output frequency fluctuations also cause inverter output power angle δ fluctuations, which cause the inverter output active power to contain power oscillations. This is not conducive to the secure and stable transmission of power in VCI grid-connected systems. According to the 3rd term in Eq. 7, the amplitude of this oscillation (f_{os}) can be calculated as:

$$f_{os} = \frac{\sqrt{2}V_{fil}(\omega_{co} - \omega_g)}{4\omega_{co}} \cdot \frac{\pi k_f}{\sqrt{1 + (2\omega_g T_f)^2}} \quad (10)$$

For eliminating the adverse effects of the oscillation, an oscillation compensation Δv_{os} is proposed as shown in Fig. 4. On the one hand, a low-pass filter (LPF) is adopted to get the accurate grid angular frequency ω_g based on Eq. 9. On the other hand, V_{fil} is replaced with a fixed v_{co} for simplifying the control method. If necessary, V_{fil} calculated in real time is used in control algorithm to achieve a more accurate control. The LPF is equal to $1/(0.01s+1)$. Therefore, Δv_{os} can be obtained as:

$$\Delta v_{os} = -\frac{\sqrt{2}\pi v_{co}(\omega_{co} - \omega_g)}{4\omega_{co}} \cos(\omega_g t + \theta) \quad (11)$$

According to the above analysis, it can be seen that compensating Δv_{os} to v_q can eliminate the adverse effects of oscillations, especially the output active power oscillation problem.

B. The Design of the Power Regulator

For making sure the VCI can connect with the grid a friendly manner, a power regulator is designed as shown in Fig. 5. In this figure, P_{set} and Q_{set} are the VCI target output active and reactive power, and $f_{fil}*$ and $V_{fil}*$ are the voltage and frequency reference for the VCI output, respectively. The coefficients of the PI controller are k_{a1}, k_{a2}, k_{b1} and k_{b2}. The coefficients k_{a3} and k_{b3} are the drooping coefficients of the active and reactive power, respectively. V_{1n} and V_{2n} as the reference axial voltage are 200 V and 0 V. In addition, ΔV_1 and ΔV_2 are the compensation amounts of the axial voltage V_1^* and V_2^*, respectively.

According to Fig.5, the VCI can output reference power precisely when the PCC voltage and frequency have no deviations. When the PCC frequency deviates from its default value, the VCI increases the reference active power through the P-f droop controller for a lower PCC frequency, whereas the VCI decrease it for a higher PCC frequency. Then through the PI controller output compensation amount ΔV_2, combined with the reference axial voltage V_{2n}, it is possible to
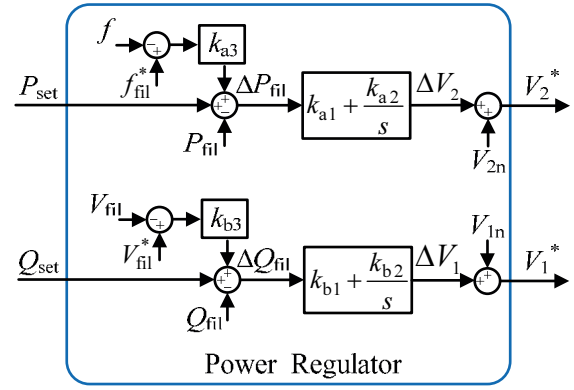

Fig. 5. Structure of the power regulator.

generate axial voltage set value V_2^*, and then send it to the axial voltage regulator and adjust the power angle δ. This has the effect of increasing or reducing the VCI active power output. Similarly, when the PCC voltage deviates from the default value, the VCI increases the reference reactive power through the Q-V droop controller for a lower PCC voltage, whereas the VCI decrease it for a higher PCC voltage. Then, through the PI controller output compensation amount ΔV_1, combined with the reference axial voltage V_{1n}, it is possible to generate axial voltage set value V_1^*, and then send it to the axial voltage regulator and adjust the equivalent voltage source amplitude. This has the effect of increasing or reducing the VCI reactive power output. On the basis of the power regulator, the VCI can automatically manage the output power with the primary frequency and voltage modulation characteristics. When the grid frequency and voltage deviate, the VCI can provide active and reactive power support to the grid during the frequency and voltage transients over a wide timeframe. The drooping coefficients k_{a3} and k_{b3} can obtained as:

$$\begin{cases} k_{a3} = \dfrac{\Delta P_{fil}}{\Delta f} \\ k_{b3} = \dfrac{\Delta Q_{fil}}{\Delta V_{fil}} \end{cases} \quad (12)$$

For designing the PI controller in a power regulator, the VCI output power characteristics are analyzed mathematically. According to Eq.1 and Eq.3, v_E and v_{fil} can be expressed as:

$$\begin{cases} v_E = \sqrt{2}V_E \sin(\omega_g t + \delta) \\ v_{fil} = \sqrt{2}V_{fil} \sin \omega_g t \end{cases} \quad \text{where } V_E = \frac{v_{co} + k_1 V_1^*}{1 + k_1} \quad (13)$$

Where V_{fil} is the voltage *rms* value [V]. According to Eq.2, Eq.13 and Fig.3., the output active and reactive power can be calculated as:

$$\begin{cases} P_{fil} = \dfrac{V_{fil}}{R^2 + X^2}[(V_E \cos \delta - V_{fil})R + V_E X \sin \delta] \\ Q_{fil} = \dfrac{V_{fil}}{R^2 + X^2}[(V_E \cos \delta - V_{fil})X - V_E R \sin \delta] \end{cases} \quad (14)$$
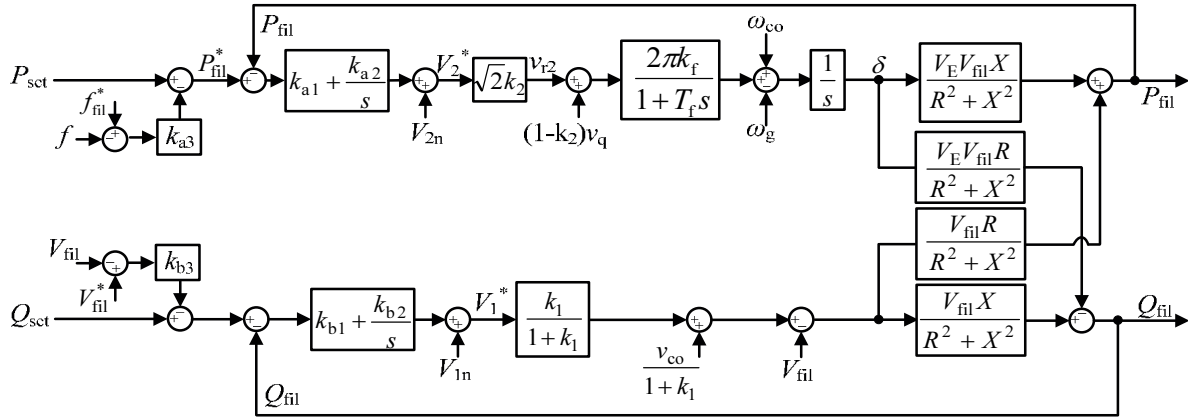
Fig. 6. Control structure of the active and reactive power loops.

Since the power angle δ is usually so small it is deemed that $\sin\delta \approx \delta$ and $\cos\delta \approx 1$. According to the control algorithm in Fig. 1, the active and reactive power loops can be obtained as shown in Fig. 6.

According to Fig. 6, the VCI reference angular frequency and voltage can be rearranged as:

$$\omega = \frac{2\pi k_f}{1+T_f s}\{\sqrt{2}k_2(k_{a1}+\frac{k_{a2}}{s})\cdot[P_{set}-P_{fil}+(f^*-f)k_{a3}]+ \tag{15}$$
$$(1-k_2)v_q\}+\omega_{co}$$

$$V_E = \frac{k_1}{1+k_1}\{(k_{b1}+\frac{k_{b2}}{s})\cdot[Q_{set}-Q_{fil}+k_{b3}(V_{fil}^*-V_{fil})]+ \tag{16}$$
$$V_{1n}\}+\frac{1}{1+k_1}v_{co}$$

Where v_q is the q axis component of v_{fil}, which is obtained by a quarter cycle delay. On the premise of $\omega_{co} \approx \omega_g$, v_q can be rearranged as:

$$v_q = -\sqrt{2}V_{fil}\delta \tag{17}$$

On the basis of the power loops, a small-signal ac model of the VCI at the quiescent operating point can be derived. It is assumed that any state variable x in these equations is equal to the corresponding quiescent value x_n, plus a superimposed small ac variation $\hat{x}$. Hence, the following equation can be obtained:

$$f = f_n + \hat{f} \tag{18a}$$

$$\omega_g = \omega_{gn} + \hat{\omega}_g \tag{18b}$$

$$\delta = \delta_n + \hat{\delta} \tag{18c}$$

$$V_E = V_{En} + \hat{V}_E \tag{18d}$$

$$V_{fil} = V_{filn} + \hat{V}_{fil} \tag{18e}$$

$$P_{fil} = P_{filn} + \hat{P}_{fil} \tag{18f}$$

$$Q_{fil} = Q_{filn} + \hat{Q}_{fil} \tag{18g}$$

$$P_{set} = P_{setn} + \hat{P}_{set} \tag{18h}$$

$$Q_{set} = Q_{setn} + \hat{Q}_{set} \tag{18i}$$

Moreover, with a proper design of the voltage control loops, the capacitor voltage can accurately track the voltage reference. Thus, the following equations can be obtained:

$$\omega_n \approx \omega_{co} \tag{19a}$$

$$V_{En} \approx V_{filn} \approx V_{fil}^* \tag{19b}$$

On the basis of equation (19a) and equation (19b), substituting equations (17), (18a), (18b), (18c), (18e), (18f) and (18h) into equation (15), and substituting equations (18d), (18e), (18g) and (18i) into equation (16), the following equations can be obtained:

$$\hat{f} = \frac{b_1 s + b_0(\hat{P}_{set}-\hat{P}_{fil}) + 2\sqrt{2}\pi(1-k_2)V_{filn}\hat{f}_g}{a_2 s^2 + a_1 s + a_o}$$
$$a_2 = \frac{T_f}{k_f}, a_1 = \frac{1}{k_f}+\sqrt{2}k_2 k_{a1}k_{a3}, \tag{20}$$
$$a_o = \sqrt{2}(2\pi(1-k_2)V_{filn}+k_2 k_{a2}k_{a3}),$$
$$b_1 = \sqrt{2}k_2 k_{a1}, b_0 = \sqrt{2}k_2 k_{a2}$$

$$\hat{V}_E = (\hat{Q}_{set}-\hat{Q}_{fil}-k_{b3}\hat{V}_{fil})\cdot\frac{k_1}{1+k_1}\frac{k_{b1}s+k_{b2}}{s} \tag{21}$$

From equation (20) and equation (21), a small-signal model between the power regulator and the VCI output voltage is established. According to equation (13), it is possible to obtain:

$$\hat{\delta} = (2\pi\hat{f}-\hat{\omega}_g)\frac{1}{s} \tag{22}$$

Based on the above calculation method of a small-signal model with equation (14), by applying the approximations $\sin\hat{\delta} \approx \hat{\delta}$ and $\cos\hat{\delta} \approx 1$, neglecting the dc terms, second and higher order ac terms, it is possible to obtain:

$$\begin{cases} \hat{P}_{fil} = \frac{V_{En}V_{filn}X}{R^2+X^2}\hat{\delta} + \frac{V_{filn}R}{R^2+X^2}(\hat{V}_E-\hat{V}_{fil}) \\ \hat{Q}_{fil} = \frac{V_{filn}X}{R^2+X^2}(\hat{V}_E-\hat{V}_{fil}) - \frac{V_{En}V_{filn}R}{R^2+X^2}\hat{\delta} \end{cases} \tag{23}$$

According to equations (20), (21), (22) and (23), a small-signal model of the power loops can be obtained as shown in Fig. 7.
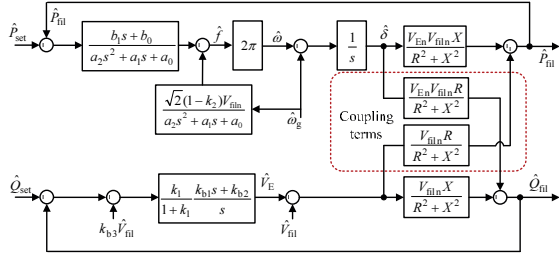
Fig. 7. Small-signal model of active and reactive power loops.
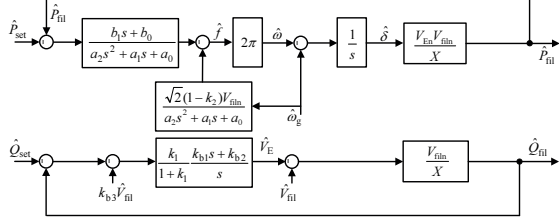

Fig. 8. Small-signal model of active and reactive power loops regardless of the coupling terms.
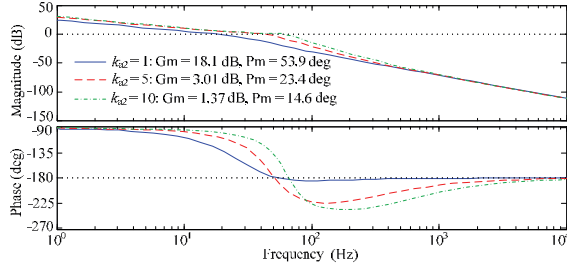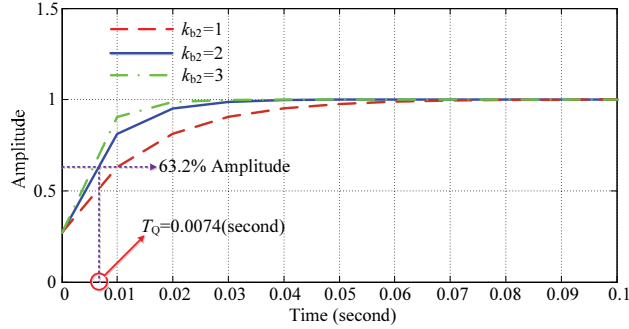

Fig. 9. Bode diagram of the active power loop gain.

Fig. 10. Step response curve of G_Q.

On the premise that the VCI inner equivalent impedance is inductive, $X \gg R$ can always be guaranteed. The coupling terms can be neglected in equation (23) and the small-signal model of the power loops can be simplified as shown in Fig. 8.

According to Fig. 8, the open-loop transfer function of the power loop can be obtained as:

$$G_P = \frac{2\pi V_{En} V_{fil}}{X} \frac{b_1 s + b_0}{a_2 s^3 + a_1 s^2 + a_0 s} \tag{24}$$

$$G_Q = \frac{k_1 V_{filn}}{(1 + k_1) X} \frac{k_{b1} s + k_{b2}}{s} \tag{25}$$

On the one hand, the control parameters k_{a1} and k_{a2} can be determined by a stability margin analysis based on equation

(24). In general, the phase margin (PM) is required in the range of $(30°, 70°)$ to achieve a good dynamic response and robustness. On the other hand, the reactive power loop is an one-order system, where the time constant T_Q determines the system dynamic performance and T_Q can be calculated by (26).

$$T_Q = \frac{k_{b1}}{k_{b2}} + \frac{(1 + k_1) X}{k_1 k_{b2} V_{filn}} \tag{26}$$

Based on the parameters in Table I, a Bode diagram of the active power loop gain can be obtained as shown in Fig. 9. This indicates that the stability margin is good for the active power loop when k_{a2} is equal to 1. With an increasing k_{a2}, the stability performance deteriorates. Meanwhile, T_Q is equal to 0.0074.

IV. SIMULATION AND EXPERIMENTAL VERIFICATION

A 200 V, 50 Hz, 1 kVA grid-connected VCI prototype was established in the Matlab/Simulink platform. The simulation step size is 0.01ms. An Ode45 is chosen as the solver, and the relative tolerance is 1e-4. The mains circuit parameters and control parameters are shown in Table I.

In order to verify that the conventional PLL output frequency has a 2 doubling frequency oscillation when the grid frequency deviates from its rated value, as well as the correctness and validity of the enhanced phase locked loop algorithm, the corresponding simulation results are shown in Fig. 11. When the PLL does not have the compensation of Δv_{os}, the VCI output frequency has a 2 doubling harmonics oscillation when the grid frequency deviated. The simulation responses are shown in Fig. 11(a). On the basis of Fig. 11(b), the oscillation is generated from v_q. With a comparison between v_q and Δv_{os}, the 2 doubling harmonics amplitude and their phases were almost equivalent. With the enhanced PLL, the VCI can track the grid frequency accurately without oscillations as shown in Fig. 11(c).

For verifying the tracking and power decoupling characteristics of the power regulator, the VCI operated with the rated grid voltage and frequency is shown in Fig. 12. The simulation was started at t = 0s. A PLL was used for the initial synchronization, which will not be discussed in this paper space limitations. For this reason, the first 0.2 s is omitted from the presented plots. The initial settings for P_{fil}^* and Q_{fil}^* were 1000 W and 0 Var. When the system is stable, a reference active power of $P_{fil}^* = 500$ W was applied with a certain slope at 0.3 s. In addition, the reference reactive power $Q_{fil}^* = 500$ Var was applied at 0.6 s.

According to Fig. 12(a), the VCI output power tracked the reference values precisely. When the VCI active power was regulated, the reactive power was almost unaffected. Meanwhile, when the VCI reactive power was regulated, the real power is almost fixed. This indicates that the VCI has an excellent decoupled power control performance. Since the

TABLE I
PARAMETERS OF THE VCI

Parameters	Values	Parameters	Values
v_{dc}	320 V	T_i	0.318 ms
L_1	5 mH	k_f	0.1 Hz/V
L_2	0.3 mH	T_f	5 ms
R_f	0.5 Ω	k_1	1.0
C_f	26.4 μF	k_2	0.5
Z_g	0.01 mH	k_{a1}	0.003
Z_{load}	40 Ω	k_{a2}	1
v_{co}	200 V	k_{a3}	1000
f_{co}	50 Hz	k_{b1}	0.006
k_{PWM}	0.995	k_{b2}	2
α	0.1	k_{b3}	100
β	-0.997	V_{fil}^{*}	200 V
γ	1.005	f^{*}	50 Hz
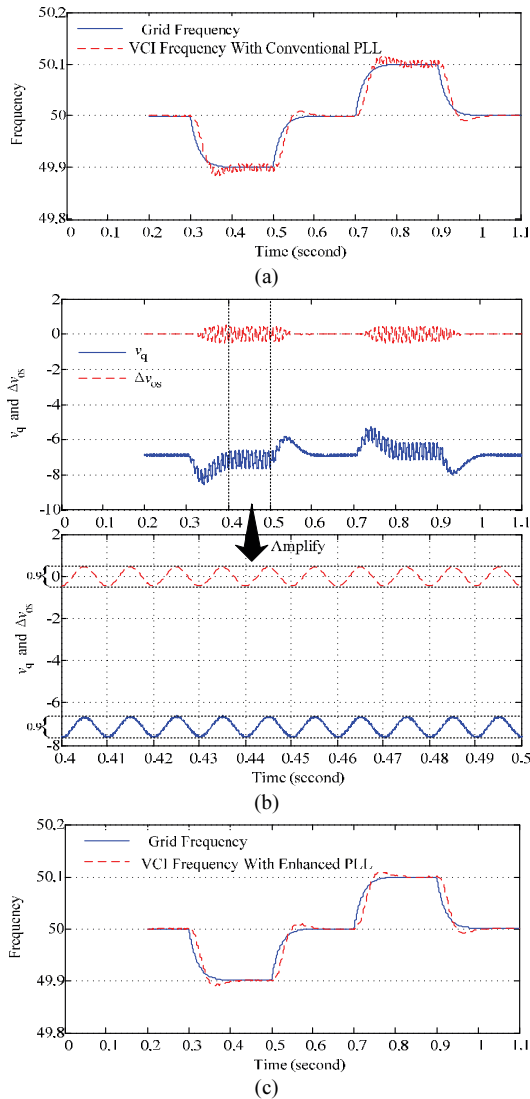
Fig. 11. Simulation results: (a) VCI output frequency and grid frequency with the conventional PLL; (b) comparison of v_q and Δv_{os}; (c) VCI output frequency and grid frequency with the enhanced PLL.
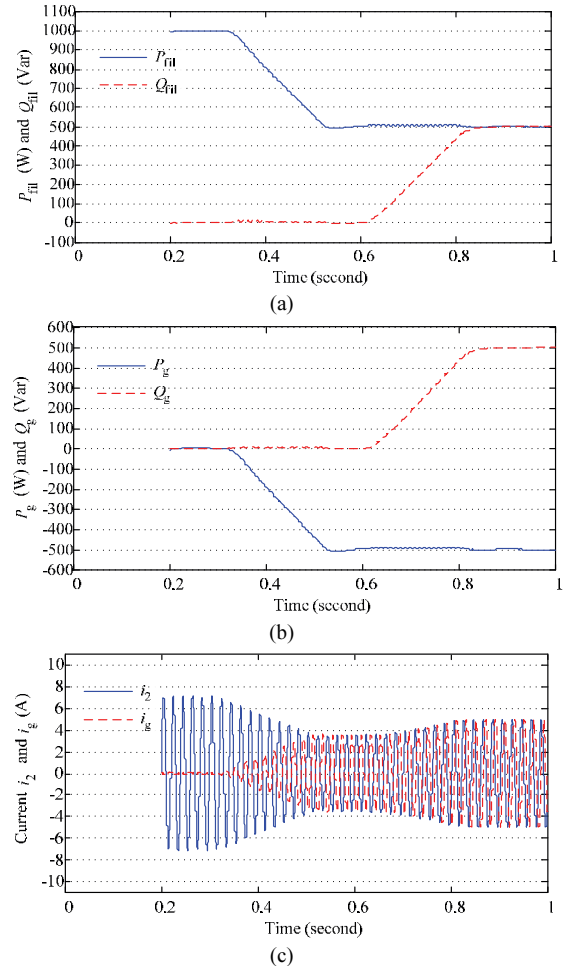

Fig. 12. Simulation results: (a) VCI output power P_{fil} and Q_{fil}; (b) grid supplying power P_g and Q_g; (c) VCI output current i_2 and grid current i_g.

load consumed approximately 1000 W, the grid provided an active power of 500 W for the load when the VCI supplied an active power of 500 W as shown in Fig. 12(b). When the VCI output 500 Var reactive power, the grid fully absorbed it. The dynamic variation between the VCI output current i_2 and the grid current i_g was shown in Fig.12(c). At the initial stage, the consumed active power of the load was fully supported by the VCI and the grid current was 0 A.

To verify the VCI primary frequency modulation characteristic, the VCI worked with the proposed power regulator as shown in Fig. 13.

The initial settings for P_{fil}^{*} and Q_{fil}^{*} were 1000 W and 0 Var. The grid frequency was varied as shown in Fig. 11(c), where the VCI output frequency accurately tracked the grid frequency. When the grid frequency varied from the nominal value to a lower one, the VCI increased a certain active power output for supporting the grid. Meanwhile, when the grid frequency varied to a higher one, the VCI decreased it. When the grid frequency was 49.9 Hz, the VCI output active power increased by 100 W, which satisfies the design based on equation (12).
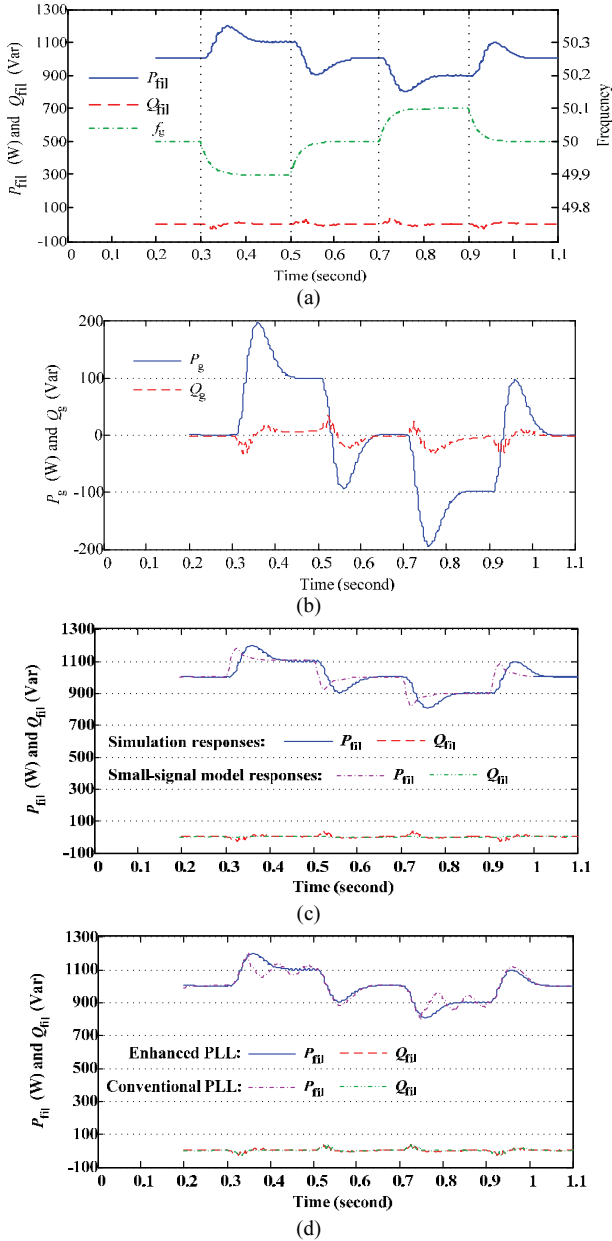
(a)

(b)

(c)

(d)

Fig. 13. Simulation results: (a) VCI output power P_{fil} and Q_{fil}; (b) grid supplying power P_g and Q_g; (c) comparison between the simulation and small-signal responses; (d) output power comparison under the conventional and enhanced PLL.

Obviously, the grid absorbed 100 W of active power when the grid frequency was 49.9 Hz as shown in Fig. 13(b). Since the simulation cannot mimic a real grid, the grid frequency cannot increase the frequency with an increasing absorption of active power. Therefore, the grid frequency was set to vary from 49.9 or 50.1 Hz back to 50 Hz. As shown in Fig. 13(a) and (b), the VCI renewed to output the reference power with active power compensation to the grid. Moreover, the VCI reactive power output is stable under a varying grid frequency. In Fig. 13(c), the responses of the small-signal model basically correspond to those of the simulation, which verifies the correctness and validity of the small-signal model.
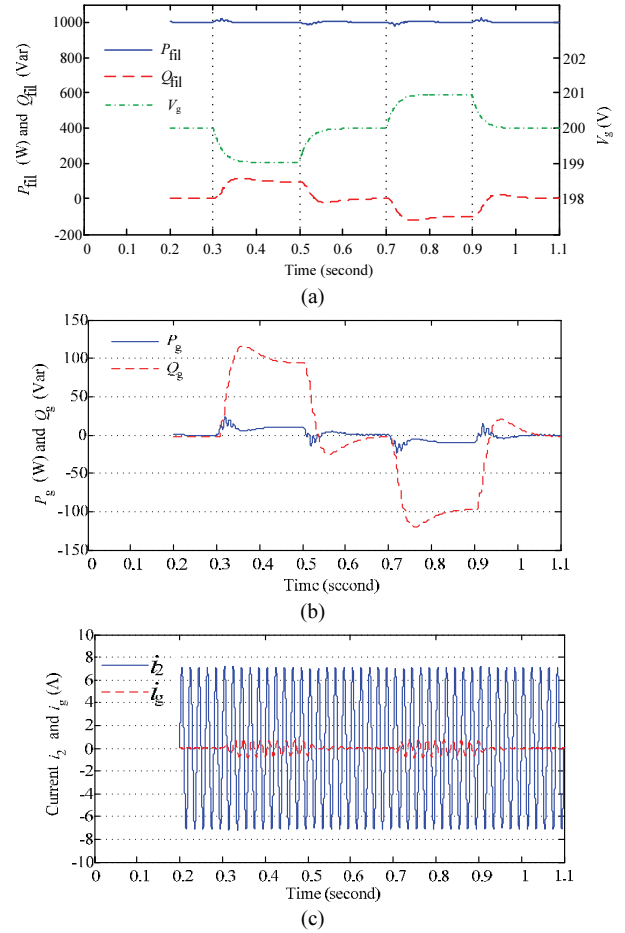

(a)

(b)

(c)

Fig. 14. Simulation results: (a) VCI output power P_{fil} and Q_{fil}; (b) grid supplying power P_g and Q_g; (c) VCI output current i_2 and grid current i_g.

The output power comparison under the conventional and enhanced PLL are shown in Fig. 13(d). When the grid frequency deviates from the rated value, there is an obvious power oscillation in the output active power of the VCI with the conventional PLL. However, when using the enhanced PLL proposed in this paper, the output active power of the VCI can be controlled smoothly. This shows that the proposed enhanced PLL can achieve a good suppression of the active power oscillation phenomenon.

The simulation results shown in Fig. 14 are given to analyze the VCI primary voltage modulation characteristic. The initial settings for P_{fil}^* and Q_{fil}^* were the same as those in Fig. 13. The initial grid voltage *rms* value was 200 V and the grid frequency was 50 Hz. A grid voltage V_g equal to 199 V was applied at 0.3 s and came back to 200 V at 0.5 s. The grid voltage varied from 200 V to 201 V at 0.7s and returned to 200 V at 0.9s.

According to Fig. 14(a), the VCI outputs reference power at the initial stage. When the grid voltage was lower than its default value, the VCI increased the reactive power output to 100Var for grid voltage support. Meanwhile, the VCI decreased reactive power output according to equation (12) at
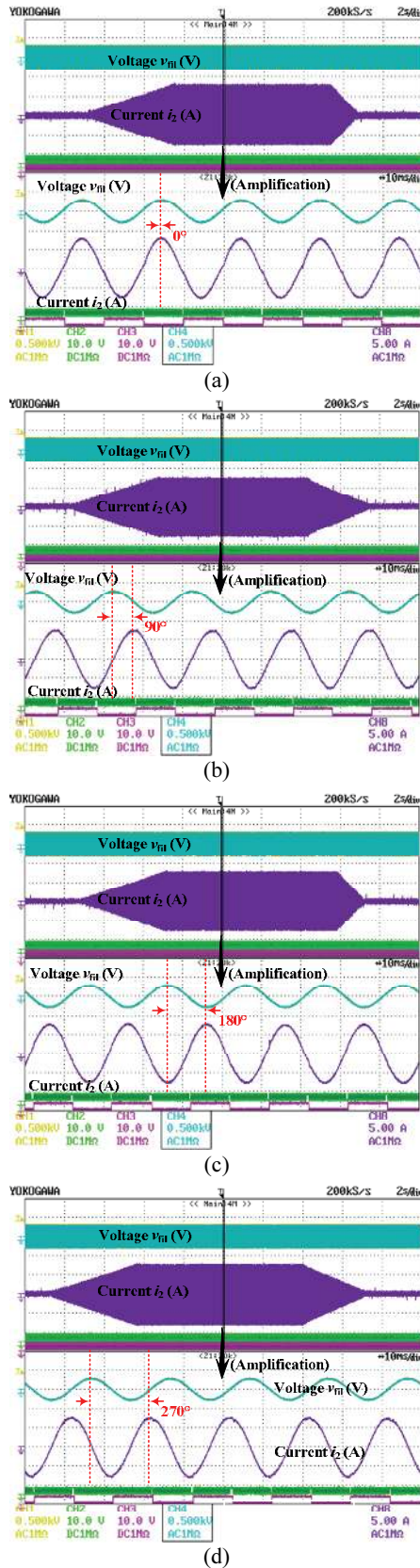
(a)

(b)

(c)

(d)

Fig. 15. Output voltage and current waveforms of grid-connected operation: (a) $P_{fil}{}^* = 1000$ W, $Q_{fil}{}^* = 0$ Var; (b) $P_{fil}{}^* = 0$ W, $Q_{fil}{}^* = 1000$ Var; (c) $P_{fil}{}^* = -1000$ W, $Q_{fil}{}^* = 0$ Var; (d) $P_{fil}{}^* = 0$ W, $Q_{fil}{}^* = -1000$ Var.
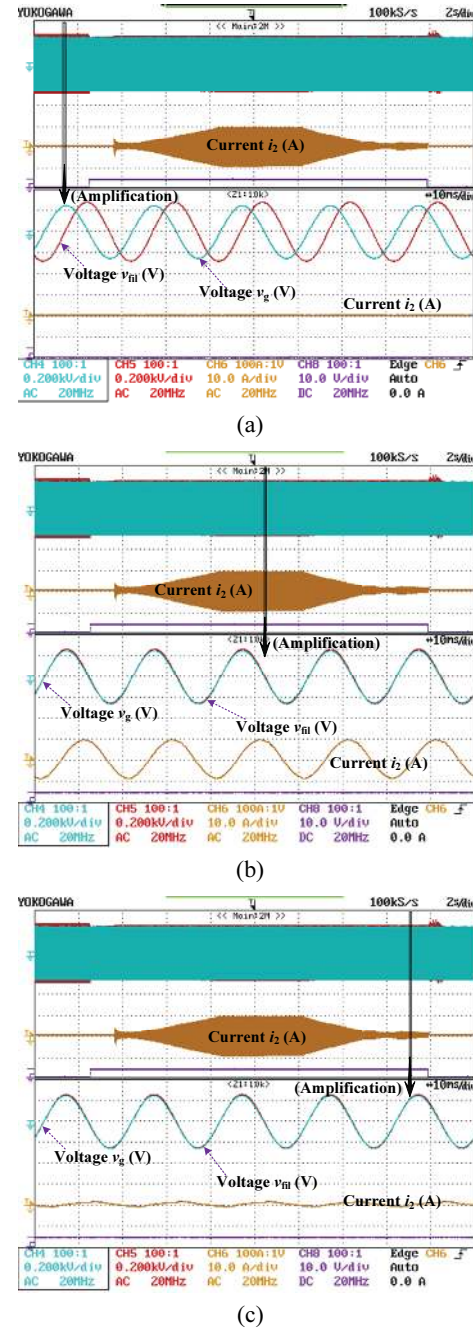

(a)

(b)

(c)
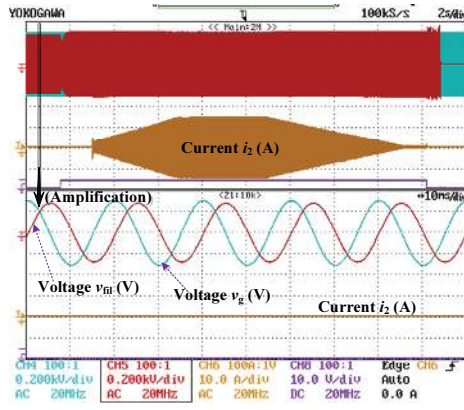
Fig. 16. Output voltage and current waveforms of grid-connected operation: (a) $V_{fil} = 200$V, $f_{fil}=50$Hz, $V_g = 180$V, $f_g=50$Hz; (b) $P_{fil}{}^* = 0$ W, $Q_{fil}{}^* = 1300$ Var; (c) $P_{fil}{}^* = 0$W, $Q_{fil}{}^* = 0$ Var.

a higher grid voltage. When the grid voltage came back to 200 V, the VCI kept 0 Var reactive power output.

To verify this idea, an experiment based on a DSP TMS320F2812 was carried out. The setup was connected with a 200 V, 50 Hz power grid through a 1:1 transformer.
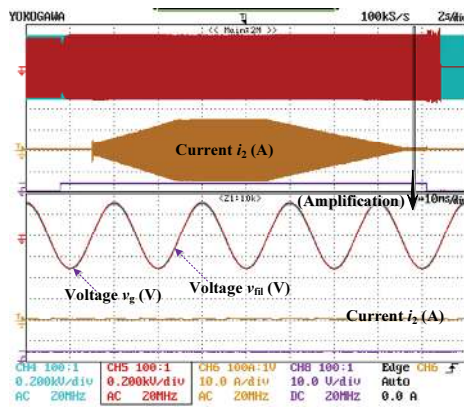
The dc voltage is set at 320 V. The time axis is 10 ms/div. The main control parameters are the same as those applied in the simulation. The rated power of the inverter is also 1kVA. On the basis of the proposed control theory, experiments were also carried out by changing the reference power $P_{fil}{}^*$
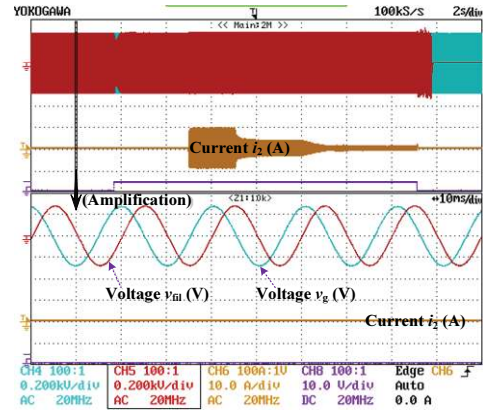
(a)
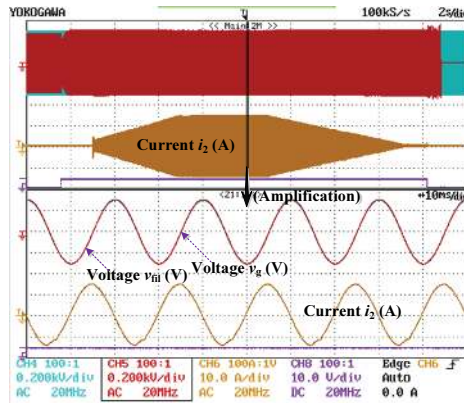
(b)

(c)

Fig. 17. Output voltage and current waveforms of grid-connected operation: (a) V_{fil}= 200V, f_{fil}=50Hz, V_g= 220V, f_g=50Hz; (b) P_{fil}^* = 0 W, Q_{fil}^* = -2300 Var; (c) P_{fil}^* =0 W, Q_{fil}^* = 0 Var.

and Q_{fil}^* as shown in Fig. 15.

According to Fig. 15, the grid-tied current i_2 is 0 with settings of (P_{fil}^*, Q_{fil}^*) = (0W, 0Var) in the initial stage. Then, the values of P_{fil}^* and Q_{fil}^* were changed to target values with a certain slope for safety reasons. When the system was stable for some time, both P_{fil}^* and Q_{fil}^* were reset to 0. The VCI can track the reference power precisely and work as a 4 quadrants machine.
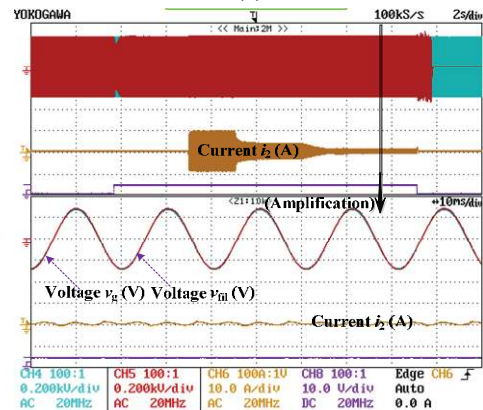
The experimental results of Fig.15 show that the PQ control strategy mentioned in this paper can realize accurate

(a)
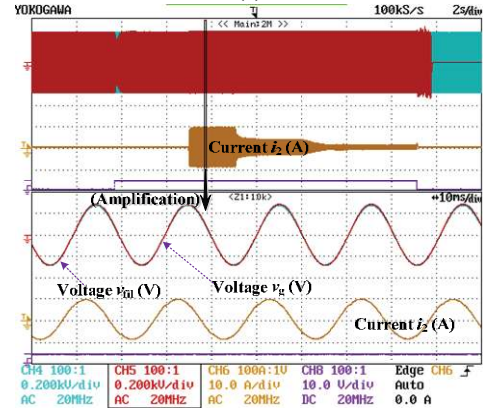
(b)

(c)

Fig. 18. Output voltage and current waveforms of grid-connected operation: (a) V_{fil}= 200V, f_{fil}=50Hz, V_g= 200V, f_g=49Hz; (b) P_{fil}^* = 1500 W, Q_{fil}^* = 0 Var; (c) P_{fil}^* = 0 W, Q_{fil}^* = 0 Var.

decoupling between the active and reactive power, and precise power control between the inverter and the grid.

The Fig. 16 and Fig. 17 show the VCI output power when the grid voltage is below and above the rated value. These figures verify that the power transmission of a VCI grid-connected system is still stable when the grid voltage deviates from its rated value.

The experimental results shown in Fig. 16 and Fig. 17 show that a VCI system can output or absorb reactive power when the grid voltage deviates from its rated value. The VCI
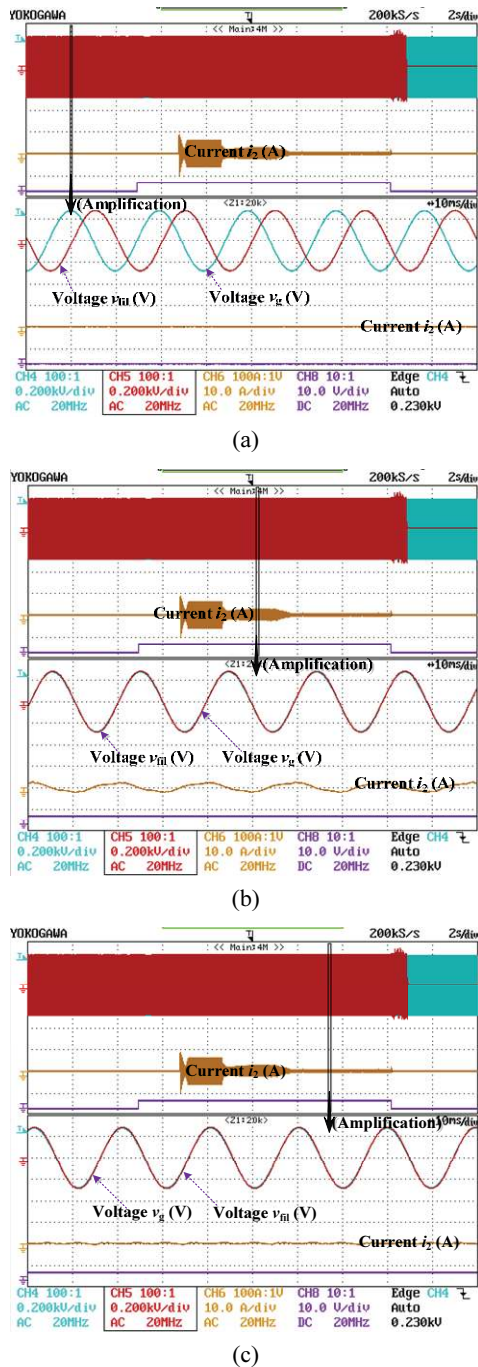
(a)

(b)

(c)

Fig. 19. Output voltage and current waveforms of grid-connected operation: (a) V_{fil}= 200V, f_{fil}=50Hz, V_g= 200V, f_g=51Hz; (b) P_{fil}^* = -300 W, Q_{fil}^* = 0 Var; (c) P_{fil}^* = 0 W, Q_{fil}^* = 0 Var.

system can provide voltage support to the grid, which makes the VCI system have a primary voltage regulation characteristic.

Fig. 18 and Fig. 19 show the VCI output power when the grid frequency is below and above its rated value, which verifies that the power transmission of the VCI grid-connected system is still stable when the grid frequency deviates from its rated value.

The experimental results shown in Fig. 18 and Fig. 19 show that the VCI system can output or absorb active power

when the grid frequency deviates from its rated value. The VCI system can provide frequency support to the grid, which makes the VCI system have a primary frequency regulation characteristic.

V. CONCLUSIONS

In this paper, a control strategy for a VCI connected with a grid is studied. In order to ensure safe and reliable operation of a VCI grid-connected system, the 2 doubling harmonics characteristics of the conventional PLL are analyzed. The 2 doubling harmonics produced by the conventional PLL cause oscillations of the output active power of the VCI. In order to solve this problem, an enhanced PLL algorithm is proposed. This algorithm can accurately output the grid frequency when the grid frequency deviates from its rated value, which can effectively suppressing oscillations of the active power. On the basis of the above analysis, to realize VCI automatic power management, the proposed power regulator with primary frequency and voltage modulation characteristics is analyzed and designed. The control parameters have been determined by establishing a small-signal model of the power loops mathematically to obtain good robustness of the system. Finally, simulation and experimental results validate this idea.

REFERENCES

[1] F. Blaabjerg, R. Teodorescu, M. Liserre, and A. Timbus, "Overview of control and grid synchronization for distributed power generation systems," *IEEE Trans. Ind. Electron.*, Vol. 53, No. 5, pp. 1398-1409, Oct. 2006.

[2] D. Zhi, L. Xu, and B. W. Williams, "Improved direct power control of grid-connected dc/ac converters," *IEEE Trans. Power Electron.*, Vol. 24, No. 5, pp. 1280-1292, May 2009.

[3] H. M. Kojabadi, B. Yu, I. A. Gadoura, L.-C. Chang, and M. Ghribi, "A novel DSP-based current-controlled PWM strategy for single phase grid connected inverters," *IEEE Trans. Power Electron.*, Vol. 21, No. 4, pp. 985-993, July 2006.

[4] F. Blaabjerg, Z. Chen, and S. Kjaer, "Power electronics as efficient interface in dispersed power generation systems," *IEEE Trans. Power Electron.*, Vol. 19, No. 5, pp. 1184-1194, Sep. 2004.

[5] L. Zhang, L. Harnefors, and H. P. Nee, "Power-synchronization control of grid-connected voltage-source converters," *IEEE Trans. Power Syst.*, Vol. 25, No. 2, pp. 809-820, May 2010.

[6] M. Ohshima and E. Masada, "A single-phase PCS with a novel constantly sampled current-regulated PWM scheme," *IEEE Trans. Power Electron.*, Vol. 14, No. 5, pp. 823-830, Sep. 1999.

[7] S.A. Khajehoddin, M. Karimi-Ghartemani, A. Bakhshai, and P. Jain, "A power control method with simple structure and fast dynamic response for single-phase grid-connected DG systems," *IEEE Trans. Power Electron.*, Vol. 28, No. 1, pp. 221-233, Sep. 2012.

[8] H. Geng, D. Xu, B. Wu, and G. Yang, "Active islanding detection for inverter-based distributed generation systems with power control interface," *IEEE Trans. Energy. Convers.*, Vol. 26, No. 4, pp. 1063-1072, Dec. 2011.

[9] S. Peng, A. Luo, Y. Chen, and Z. Lv, "Dual-loop power control for single-phase grid-connected converters with LCL filter," *J. Power Electron.*, Vol. 11, No. 4, pp. 1-8, Jul. 2011.

[10] M. Ashabani, Y. Mohamed, M. Mirsalim, and M. Aghashabani, "Multivariable droop control of synchronous current converters in weak grids/microgrids with decoupled dq-axes currents," *IEEE Trans. Smart Grid*, Vol. 6, No. 4, pp. 1610-1620, Jul. 2015.

[11] T. L. Vandoorn, B. Renders, and L. Degroote, "Active load control in islanded microgrids based on the grid voltage," *IEEE Trans. Smart Grid*, Vol. 2, No. 1, pp. 139-151, Mar. 2011.

[12] Q.-C. Zhong and G. Weiss, "Synchronverters: Inverters that mimic synchronous generators," *IEEE Trans. Ind. Electron.*, Vol. 58, No. 4, pp. 1259-1267, Apr. 2011.

[13] Q.-C. Zhong, P. L. Nguyen, Z. Ma, and W.-X. Sheng, "Self-synchronized synchronverters: inverters without a dedicated synchronization unit," *IEEE Trans. Power Electron.*, Vol. 29, No. 2, pp. 617-630, Feb. 2014.

[14] Y. Li and Y. W. Li, "Power management of inverter interfaced autonomous microgrid based on virtual frequency-voltage frame," *IEEE Trans. Smart Grid*, Vol. 2, No. 1, pp. 30-40, Mar. 2011.

[15] A. Luo, Y.-D. Chen, Z. K. Shuai and C.-M. Tu, "An improved reactive current detection and power control method for single-phase photovoltaic grid-connected DG system," *IEEE Trans. Energy. Convers.*, Vol. 28, No. 4, pp. 823-831, Nov. 2013.

[16] X. Tang, K. M. Tsang, and W. L. Chan, "A power quality compensator with DG interface capability using repetitive control," *IEEE Trans. Energy. Convers.*, Vol. 27, No. 2, pp. 213-219, Jun. 2012.

[17] A. Cagnano, E. De Tuglie, M. Liserre, and R. A. Mastromauro, "Online optimal reactive power control strategy of PV inverters," *IEEE Trans. Ind. Electron.*, Vol. 58, No. 10, pp. 4549-4558, Oct. 2011.

[18] D. Yazdani, M. Mojiri, A. Bakhshai, and G. Joós, "A fast accurate synchronization technique for extraction of symmetrical components," *IEEE Trans. Power Electron.*, Vol. 24, No. 3, pp. 674-684, Mar. 2009.

[19] R. A. Mastromauro, M. Liserre, T. Kerekes, and A. D. Aquila, "A single phase voltage-controlled grid-connected photovoltaic system with power quality conditioner functionality," *IEEE Trans. Ind. Electron.*, Vol. 56, No. 11, pp. 4436-4444, Nov. 2009.

[20] R. Bojoi, L. Limongi, D. Roiu, and A. Tenconi, "Enhanced power quality control strategy for single-phase inverters in distributed generation systems," *IEEE Trans. Power Electron.*, Vol. 26, No. 3, pp. 798-806, Mar. 2011.

[21] G. Franceschini, E. Lorenzani, and G. Buticchi, "Saturation compensation strategy for grid connected converters based on line frequency transformers," *IEEE Trans. Energy Convers.*, Vol. 27, No. 2, pp. 229-237, Jun. 2012.

[22] P. Rodriguez, J. Pou, J. Bergas, J. I. Candela, R. P. Burgos, and D. Boroyevích, "Decoupled double synchronous reference frame PLL for power converters control," *IEEE Trans. Power Electron.*, Vol. 22, No. 2, pp. 584-592, Mar. 2007.

[23] R. Santos Filho, P. Seixas, P. Cortizo, and A. Souza, "Comparison of three single-phase PLL algorithms for UPS applications," *IEEE Trans. Ind. Electron.*, Vol. 55, No. 8, pp. 2923-2932, Aug. 2008.

[24] Q. Zhang, X.-D. Sun, Y.-R. Zhong, M. Matsui, and B.-Y. Ren, "Analysis and design of a digital phase-locked loop for single-phase grid-connected power conversion systems," *IEEE Trans. Ind. Electron.*, Vol. 58, No. 8, pp. 3581-3592, Aug. 2011.

[25] T. Thacker, D. Boroyevich, R. Burgos, and F. Wang, "Phase-locked loop noise reduction via phase detector implementation for single-phase systems," *IEEE Trans. Ind. Electron.*, Vol. 58, No. 6, pp. 2482-2490, Jun. 2011.

[26] J. Zhao, S. Ushiki, and M. Ohshima, "Grid-connected inverter with inner output impedance and governor-free characteristics," *IEEE Energy Conversion Congress and Exposition (ECCE)*, pp. 586-593, 2010.

Jia-Yuan Gao was born in Henan, China, in 1991. He received his B.S. degree in Electrical Engineering from the Henan Polytechnic University, Henan, China, in 2015. He is presently working towards his M.S. degree at the Shanghai University of Electric Power, Shanghai, China. His current research interests include grid-connected inverter control and stability control of renewable energy power generation systems.

Jin-Bin Zhao (M'06) was born in Hubei, China, in 1972. He received his M.S. and Ph.D. degrees in Electrical Engineering from Oita University, Oita, Japan, in 2002 and 2005, respectively. He worked as a Researcher in the R&D Headquarters of the Origin Electric Co., Ltd., Tokyo, Japan, from 2005 to 2011. He is presently working as a Professor at the Shanghai University of Electric Power, Shanghai, China. His current research interests include the control of power converters, soft-switching power converters, inverters, distributed power systems, power-factor correction, and electric drive systems. Dr. Zhao is a Member of the IEEJ and IEICE of Japan as well as a Senior Member of the CPSS.

Chao-Jie He was born in Zhejiang, China, in 1990. He received his B.S. degree in Electrical Engineering and Automation from Hangzhou Dianzi University, Zhejiang, China, in 2013. He is presently working towards his M.S. degree in Electrical Engineering at the Shanghai University of Electric Power, Shanghai, China. His current research interests include grid-connected inverter control and renewable energy generation systems.

Shuaitao Zhang was born in Henan, China, in 1990. He received his B.S. degree in Electrical Engineering from the North China University of Water Resources and Electric Power, Henan, China, in 2013. He is presently working towards his M.S. degree at the Shanghai University of Electric Power, Shanghai, China. His current research interests include the modeling and analysis of inverters and grid-connected control of renewable energy power generation.

Fen Li received her B.S. and Ph.D. degrees in Electrical Engineering from the Huazhong University of Science and Technology, Wuhan, China, in 2005 and 2010, respectively. She has been working as an Engineer in the Hubei Meteorological Bureau, Wuhan, China, since 2010. She is presently working as a Lecturer at the Shanghai University of Electric Power, Shanghai, China. Her current research interests include high power factor converters, grid-connected control of renewable energy power generation, solar resource evaluation and forecast, the relationship between photovoltaic power and meteorological factors, and PV power prediction.